Thermal Science and Engineering Progress 72 (2026) 104614

Contents lists available at ScienceDirect

Thermal Science and Engineering Progress

journal homepage: www.sciencedirect.com/journal/thermal-science-and-engineering-progress

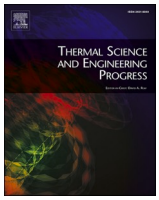

Thermo-fluid dynamic analysis of a cooling system for an inclined plate

Alfredo Pagliaro [a,*], Francesco Braghin [a], Francesco Devia [b], Gregorio Giannini [a], Vittoria Malaman [a], Francesco Miselli [c]

[a] Politecnico di Milano, Department of Mechanical Engineering, Via Giuseppe La Masa 1, Milano 20156, Italy
[b] Università degli Studi di Genova, DIME, V. all'Opera Pia, 15A, 16145 Genova, Italy
[c] Fincantieri S.p.a, Naval Vessels Division, Engineering & Design, Via Cipro 11, 16129 Genova, Italy

ARTICLE INFO

Keywords:
Heat sink
CFD
VOF
Fluid film
Cooling system
Heat transfer

ABSTRACT

Inclined plates equipped with nozzle systems for wall cooling and cleaning are employed in a wide range of industrial applications, including the metallurgical, nuclear, energy, and marine sectors. Although jet-based cooling has been widely investigated, detailed multiphase simulations are often computationally expensive and difficult to validate experimentally. In this context, a detailed investigation of the thermo-fluid dynamic behavior of the jet distribution, impact, and plate cooling process is essential. In this study, Computational Fluid Dynamics (CFD) simulations were performed to accurately capture the physics of the problem and realistically predict the resulting flow and heat transfer phenomena.

The aim of this work is twofold: first, to analyze in detail different physical modeling approaches, ranging from a simplified one-dimensional model to a more compact and comprehensive one that accounts for jet dynamics; second, to compare the obtained results to assess the robustness of an intermediate model representing the optimal trade-off between computational cost and accuracy. Finally, the numerical predictions were validated against experimental data, showing maximum temperature deviations below 1.31°C and mean absolute errors lower than 0.79°C. This demonstrates that a simplified CFD approach can reliably reproduce the thermal behavior of more complex multiphase models while significantly reducing the computational cost. This contribution provides a validated and efficient methodology for thermal analysis and design of jet-cooled inclined surfaces at engineering scale.

1. Introduction

Computational fluid dynamics (CFD) simulations play a key role in the design and optimization of cooling and washing systems across a wide range of engineering sectors, including energy production, nuclear engineering, aerospace, and naval applications [1]. By providing a detailed insight into the complex interactions between fluid flow and heat transfer, this approach allows for an in-depth investigation of the governing physical equations, facilitating accurate and realistic predictions of system behaviour under varying operational conditions [1]. The strict integration among experimental activities and CFD analysis is the key for increasing test results comprehension and widening the knowledge to aspects that can hardly be measured but can be calculated with CFD. In this work, the analysis is focused on evaluating the thermodynamic equilibrium of an inclined plate subjected to solar heat flux and actively cooled by a dedicated nozzle system spraying water. The inclined plate and its associated cooling configuration have multiple practical applications, including fluid-film heat exchangers, the cleaning of solar panels, the cooling of metallic surfaces following casting or rolling processes, and the washing of naval bulkheads [2,3]. The study not only considers the thermal distribution on the plate but also investigates the detailed fluid dynamic behaviour of the impinging water jet, including its spreading, impact characteristics, and wettability on the surface. To achieve this, the problem was approached using both an analytical methodology, solving the governing physics equations, and a comprehensive numerical simulation capable of capturing the intricate details of heat transfer and free-surface dynamics [4]. Based on the above considerations, the present work is motivated by the need for accurate and computationally efficient thermo-fluid dynamic models for the analysis of jet-cooled inclined surfaces under realistic operating conditions. The study investigates the cooling of an inclined plate subjected to solar irradiation by combining experimental measurements

* Corresponding author.
E-mail address: alfredo.pagliaro@polimi.it (A. Pagliaro).

https://doi.org/10.1016/j.tsep.2026.104614
Received 14 January 2026; Received in revised form 20 February 2026; Accepted 27 February 2026
Available online 28 February 2026
2451-9049/© 2026 The Authors. Published by Elsevier Ltd. This is an open access article under the CC BY license (http://creativecommons.org/licenses/by/4.0/).

with numerical simulations. Different modelling strategies are analysed, ranging from a simplified one-dimensional approach to three-dimensional CFD simulations, including both a fluid film model and a detailed multiphase VOF formulation. The numerical results are systematically compared and validated against experimental data obtained on a full-scale inclined plate.

The main novelty of this work lies in the experimental validation and quantitative comparison of CFD models of different complexity, demonstrating that a simplified fluid film approach can accurately reproduce the thermal behaviour of a computationally expensive multiphase VOF model while significantly reducing the computational cost. The main contributions of the present study can be summarized as follows:

- development and comparison of thermo-fluid dynamic models of increasing complexity for jet-cooled inclined plates;
- experimental validation of the proposed CFD approaches under realistic operating conditions;
- identification of an efficient and reliable modelling strategy suitable for engineering-scale thermal analyses.

2. State of the art

Spray systems and impingement jet cooling have been extensively investigated as effective techniques for enhancing heat transfer on inclined surfaces, heat sinks, and in industrial applications such as solar energy systems and metallurgical processes. The performance of these cooling techniques is greatly influenced by both geometric parameters and flow conditions. In recent years, optimization strategies, multi-jet configurations, and CFD-based validation approaches have attracted significant interest from researchers [5,6]. In some studies, the Taguchi method is employed to enhance heat transfer in inclined multi-jet impingement cooling systems applied to rectangular finned heat sinks for electronic devices [7]. The optimized configuration achieved a 28.61% improvement in heat transfer compared to the flat place. Then, the optimized geometry was further examined through numerical and experimental studies, considering different impingement jet velocities, nozzle diameters and heat flux values, demonstrating good agreement between simulations and experiments [8,9]. While geometric optimization has been shown to significantly enhance cooling performance, heat transfer and flow characteristics remain key governing factors. In particular, the influence of droplet size distribution, spray cone angle, nozzle pressure, and impingement angle on cooling efficiency and surface temperature uniformity has been widely reported in previous studies [6,10]. Nevertheless, existing studies on jet impingement and spray cooling mainly consider either simplified flat surfaces or optimized heat sink geometries, typically assuming horizontal orientations and neglecting gravitational effects on liquid film development [11]. Furthermore, many numerical models rely on either purely analytical correlations or fully resolved CFD simulations, which can be computationally expensive and difficult to integrate into early-stage engineering design workflows. In this context, the present work addresses the heat transfer phenomenon on an inclined plate actively cooled by a nozzle-generated water jet, explicitly accounting for gravitational effects on jet spreading, liquid film formation, and surface wettability. Furthermore, the adoption of a VOF-based numerical framework enables realistic prediction of liquid film thickness, jet impact region, and surface coverage, which are often neglected or oversimplified in conventional impingement cooling studies. A hierarchical modelling strategy is adopted, ranging from a simplified one-dimensional analytical model to a compact CFD-based approach. This methodology allows an evaluation of the predictive capability of intermediate-fidelity models, together with the identification of an optimal balance between computational cost and physical accuracy.

3. Scope of the work

The aim of this work is the fluid-dynamic and thermal analysis of a plate subjected to solar irradiation and actively cooled. The cooling system is designed to distribute water as evenly as possible across the surface, ensuring uniform cooling across the entire wetted surface [12]. Achieving uniform distribution increases the likelihood of removing dirt and therefore achieving a better final surface cleaning. The plate geometry used for this discussion was created in SolidWorks based on realistic dimensions; as shown in Fig. 1, the geometry taken as a reference for the test case presents a width (W) of 0.5 m, a length of 2.5 m, a thickness (t) of 5 mm and an inclination of 45°. In addition, the inclination angle was set to 45° in order to faithfully replicate the geometry of the real plate and to validate the CFD results against experimental data. Indeed, due to the high computational cost, particularly for the multiphase VOF simulations, the numerical analyses were carried out by reproducing the real operating conditions as closely as possible. Moreover, the Tab. 1 shows the thermodynamic properties of the plate material and water; these values were extracted from the database used in the software for the computational calculations [13].

In addition, the plate features a nozzle positioned on the top surface, used to spray water as a cooling fluid in order to ensure a homogeneous distribution, uniform cooling, and washing. The nozzle geometry, shown in Fig. 2, was modelled in SolidWorks based on the actual geometry of the experimental setup. A water jet nozzle with an outlet diameter of 3.6 mm was used in the study, corresponding to the nozzle installed in the experimental setup. This configuration was selected to ensure a uniform water distribution on the plate and to enable a direct validation of the CFD results against experimental data.

The thermo-fluid dynamic problem was primarily addressed through computational fluid dynamics (CFD) simulations using STAR-CCM + software [13].

Three different approaches were used to analyse the problem:

- One-dimensional model based on the solution of fluid-dynamic and thermodynamic equations, discretized in time and space using MATLAB [4,14].
- Simplified computational model in STAR-CCM+, using a fluid film to replicate the water flowing and wetting the plate.

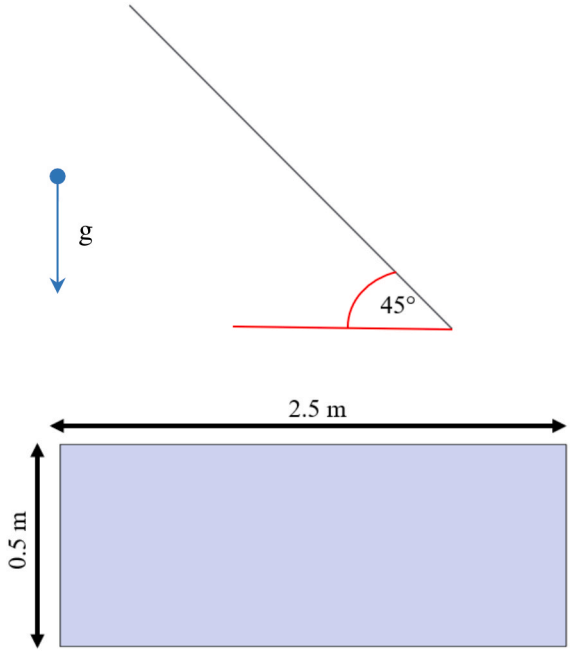

Fig. 1. Plate dimensions and inclination.

Table 1
Thermodynamic properties of the plate and the fluid [13].

Thermodynamic properties	Stainless Steel	Water (25°C)
Density [kg/m^3]	8055	997.561
Specific heat [J/kg • K]	480	4181.72
Thermal conductivity [W/m • K]	15.1	0.620271
Dynamic viscosity [Pa • s]	/	8.8871e^{-4}

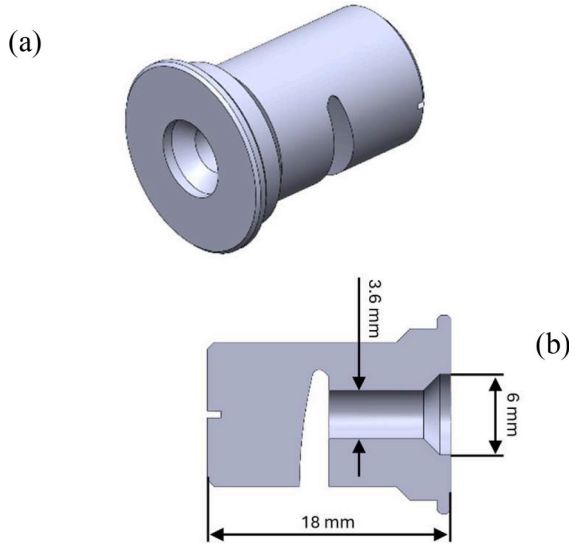

Fig. 2. (a) Nozzle geometry. (b) Section of the nozzle.

- Detailed computational model in STAR-CCM + including the nozzle, thus implementing a three-dimensional fluid model that accounts for jet distribution and the turbulence involved [15].

Finally, these models were not only compared with each other but also validated against experimental data obtained from the tests, thus achieving the validation of the developed computational model. Indeed, the ultimate goal of this study is to develop a thermal analysis based on solar flux shielding, while identifying a thermo-fluid dynamic compromise for the design and thermo-hydraulic verification of large plates. Since the jet impingement is not the crucial aspect in this context, the goal is to establish a model that is as simple as possible but sufficiently accurate. In this way, the thermal results obtained from a simplified model could accurately approximate those of a detailed study that takes into account the multiphase physics of the problem, thus enabling the computational investigation of various geometries under different operating conditions.

4. Fluid-dynamic analysis

4.1. One-dimensional Fluid-Dynamic model

The one-dimensional model of the heat transfer from the plate to a cooling film of water, driven by buoyancy, represents the simplest calculation presented in this analysis. It approximates the entire plate as a one-dimensional structure, assuming that the temperature along the midline of the plate is uniform across its width. In this way, the goal is to study the spatial and temporal discretization of how the temperature evolves along that centerline as water flows over the plate [16]. Therefore, the characteristic reference dimension is the length of the plate subjected to a constant solar heat flux, allowing the study of temperature evolution over time and along the spatial domain. Moreover, since the thickness is much smaller than the characteristic dimension, the problem can be approximated by a lumped-parameter analysis, assuming that the temperature variation across the thickness is negligible [4].

The energy balances for the heat transfer of the plate and the water were formulated as follows [4]:

$$\rho c_{p,plate} s \frac{\partial T_p}{\partial t} = k \frac{\partial^2 T_p}{\partial x^2} + q'' - h\left(T_p - T_w\right) \quad (1)$$

$$\dot{m} c_{p,\,water} \frac{dT_w}{dx} = hW\left(T_p - T_w\right) \quad (2)$$

The energy balance for the plate, shown in Eq. (1), accounts for a conductive term represented by the second-order derivative, a convective term due to heat exchange with the water, and finally the solar heat flux. The energy balance for the water shown in Eq. (2), on the other hand, considers a spatial convective term and the heat exchanged between the plate and the water. These equations are discretized both in time and space and solved on MATLAB. Specifically, the water temperature is solved by discretizing the equation along the spatial component. This temperature is then used to solve the temperature distribution for the plate, which also depends on a temporal component, as a constant heat flux acts on the structure [4,12].

The boundary conditions were chosen consistently with those used in subsequent CFD analyses and with the test facilities The water flow rate is selected so as to ensure fluid-dynamic similarity with the data used to conduct the real experiments, corresponding to a Reynolds number of approximately 50,000 and an initial water temperature of 24°C, while the initial plate temperature is set to 30°C [12,17]. For the solar flux, the plate is designed with a coating capable of reflecting part of the incident thermal power; therefore, the reference value is set to 570 W/m^2. The same water thermophysical properties were used for both the 1D and Star-CCM + simulations. The time series of temperature profiles along the plate, calculated by 1D model, is plotted in Fig. 3 [16]. Finally, it is possible to graphically represent this temperature field, assuming uniform values across the entire width of the plate. Fig. 4 shows the temperature field for the plate under study [18].

4.2. Simplified three-dimensional computational fluid dynamics model

The first computational fluid dynamics (CFD) analysis was performed by simplifying the problem through the adoption of a thin-film model. The software used was STAR-CCM+, which allows the implementation of the shell option, enabling the simulation of a two-dimensional thin-film fluid model and thus neglecting the three-dimensional discretization of the water flow [13,19]. This approach significantly reduces the computational cost, avoiding the need for more complex models such as three-dimensional Volume of Fluid (VOF) simulations [15].

In this model, air was defined as the primary medium, while water was introduced as a secondary thin-film phase. Since the ambient air conditions were not known, both forced and natural air convection were neglected in this work, focusing instead on the heat exchange between the water and the plate and the surface distribution of water. This assumption ensures consistency with the results obtained in the previous section [4]. Accordingly, the automatic thermal contact between the two fluids was disabled in the model, thus excluding the influence of air in the overall heat transfer balance. The computational model was approximated as a laminar flow case, and gravity was introduced into the system to realistically account for the downward motion of the liquid along the wall. The boundary conditions are the same defined previously: a mass flow rate sufficient to ensure a Reynolds number of approximately 50,000 with a temperature of 24°C, while the initial temperature of the plate is set to 30°C [12,17]. As a reference case, it has been assumed the combination of solar radiation and plate coating emissivity correspond to an absorbed heat flux of 570 W/m^2. The thickness of the thin film of water is very small and its contribution to

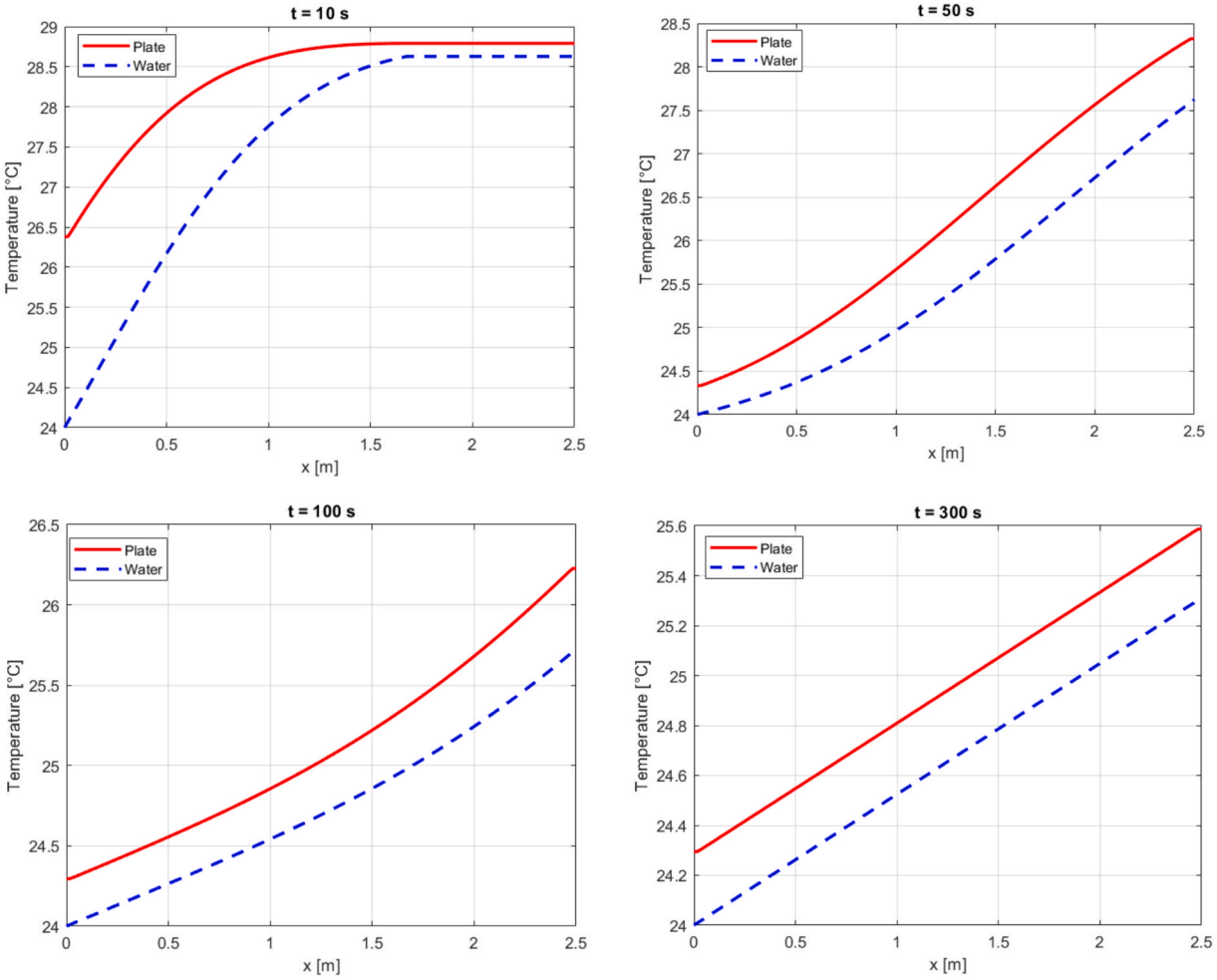

Fig. 3. Temporal evolution of the plate and water temperature along the spatial dimension.

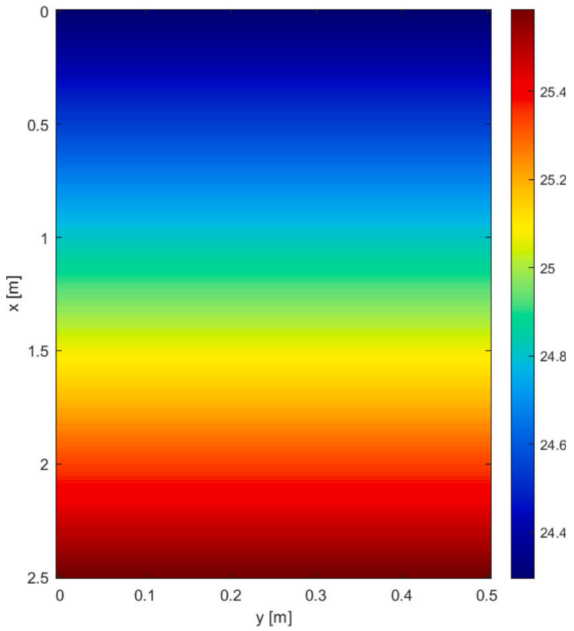

Fig. 4. Steady-state temperature distribution of the plate obtained from MATLAB.

absorption of solar radiation can be neglected, therefore a unique value of absorbed solar radiation can be used for both wet and dry plate. This specified value is applied to the surface exposed to solar radiation, while all other surfaces are considered adiabatic. For the mesh, since STAR-CCM + solves the governing equations using the finite volume method, a polyhedral mesh was adopted, which provides higher accuracy compared to triangular or quadrilateral elements [13,15]. As shown in Fig. 5, the plate thickness, being very thin, was treated using a thin layer approach, with a sufficient number of layers to ensure proper heat transfer. Finally, the inlet region was refined to accurately capture potential flow instabilities [15]. Moreover, to ensure the reliability of the numerical results, a mesh independence study was performed. Several meshes with progressively increasing resolution were tested, and the resulting temperature values were compared. The results, summarized in Tab. 2, present the absolute temperature variation (ΔT) and the corresponding relative difference (%) between the i-th mesh and the finest one. The negligible variations observed with further refinement confirm the mesh independence of the solution.

The idea of approximating the model as a thin-film fluid stems from the need to reduce the computational time, which would otherwise be very demanding due to both the geometric dimensions involved and the complexity of the three-dimensional physics of the problem. The main idea was to neglect the initial jet distribution generated by the water spray at the nozzle, focusing instead on the central region of the flow, where water flows downward along the wall, forming a liquid film and cooling the surface [19].

To ensure consistency with the physical characteristics of the nozzle, in the software the film thickness was set to obtain flow velocities

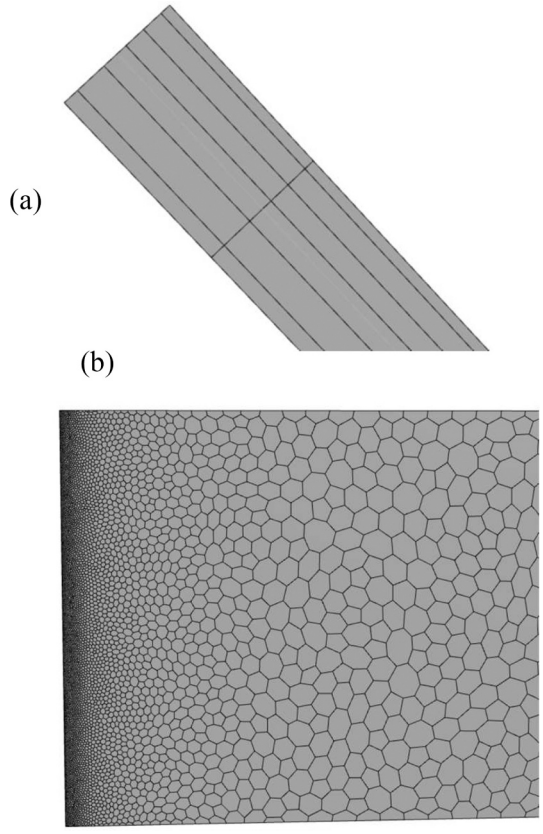

Fig. 5. Mesh setup of the geometry for the CFD simulation. (a) Side view. (b) Front view.

Table 2
Mesh independence analysis based on the point temperature value, the absolute difference, and the corresponding relative temperature variation between the i-th mesh and the finest one.

Mesh	T (point) [°C]	ΔT[°C]	ΔT[%]
Coarse	24.94	0.17	0.68
Medium	24.96	0.15	0.59
Fine	25.07	0.04	0.15
Extra-Fine	25.11	0.00	0.00

comparable to those expected during the spray phase. Indeed, by considering the specific mass flow rate and the characteristic dimension (diameter) of the nozzle, it is possible to estimate the water flow velocity. Furthermore, knowing the total width of the panel, it is possible to determine the hypothetical film thickness of $2.04e^{-5}$ m that would yield the same expected velocity at the nozzle outlet.

One of the objectives of the transient analysis was the estimation of the time required for the system to reach steady-state conditions. Indeed, one of the future goals is the development of a control system capable of regulating the mass flow rate as a function of the target temperature to be achieved on the plate.

Fig. 6 shows the thermal profile along the plate [18].

Additionally, the graph shown in Fig. 7 depicts the temperature evolution along the centerline of the plate [15].

The figures show that the temperature field increases almost linearly. Specifically, the plate, subjected to a constant heat flow, gradually heats up over time while being simultaneously cooled by water. The water, in turn, heats up along the length of the plate, thus causing an almost linear increase in the temperature of the plate. This behavior becomes more pronounced as the plate length increases: the longer the plate, the more the water absorbs heat and warms up, thereby reducing its cooling effect

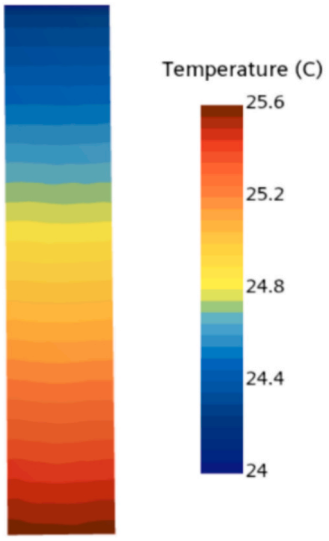

Fig. 6. Steady-state temperature distribution along the plate.

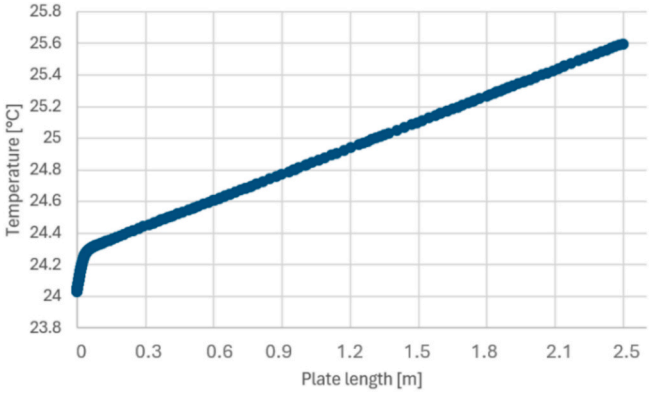

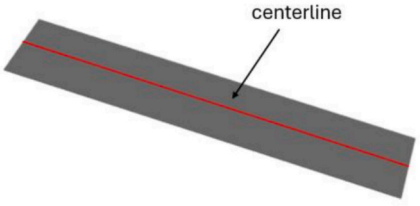

Fig. 7. Steady-state temperature profile along the centerline of the plate.

on the plate at the farthest point. Moreover, Fig. 8 shows the residual plots and the time evolution of the pointwise temperature at the bottom of the plate once convergence has been reached. This criterion was adopted as the convergence criterion for all CFD analyses.

Finally, since this is a transient simulation, it is possible to estimate the time required for the entire structure to reach steady state. Looking at time evolution of the temperature profile, it is evident that steady-state conditions are reached after 190 s. Moreover, the temperature fields obtained from the two computational (1D and fluid-film) approaches exhibit almost identical results, further confirming the robustness of the model. Minor discrepancies in the temporal and thermal results are acceptable and can be attributed to the actual fluid-dynamic history, which is also influenced by inclination and gravity.

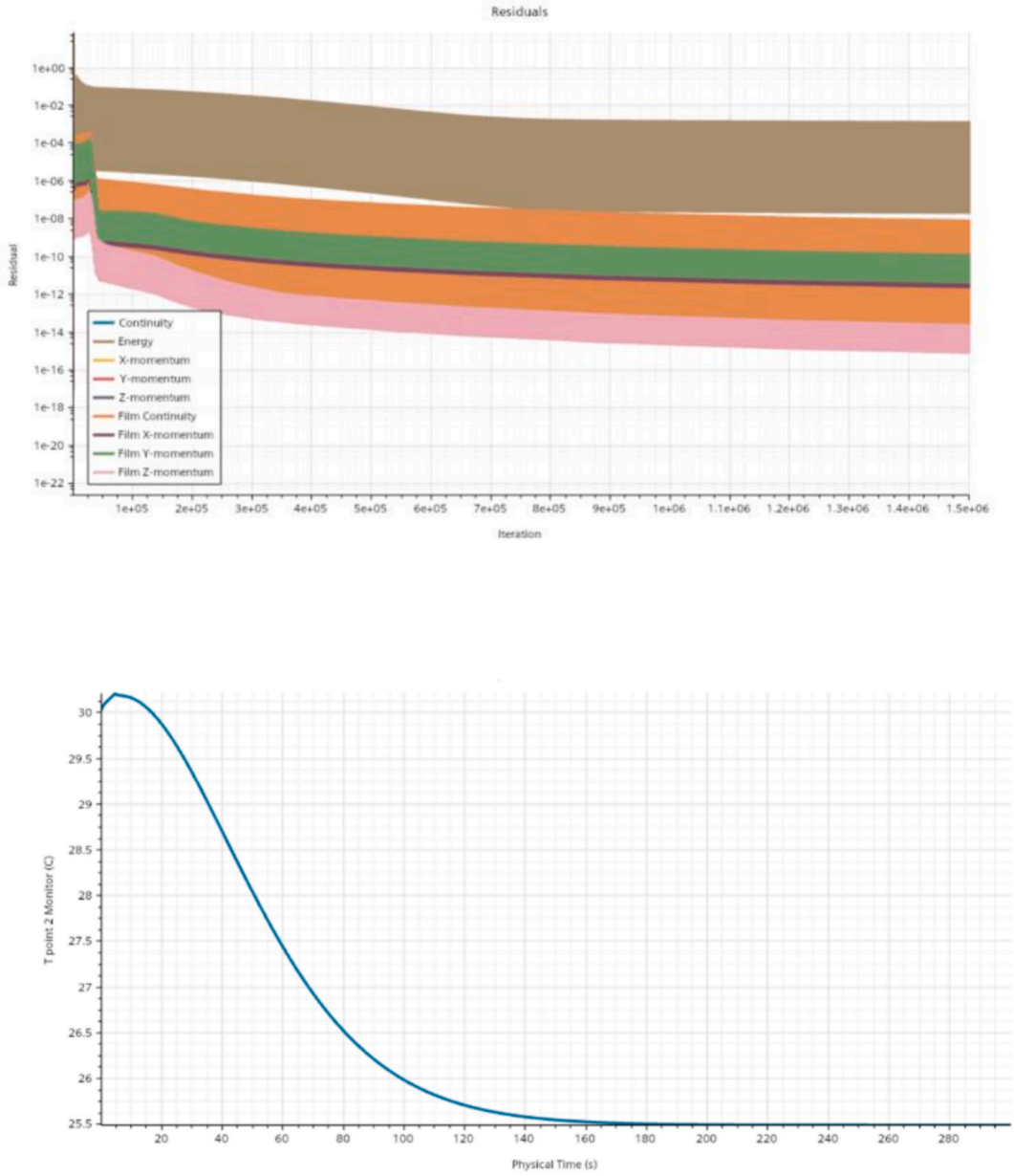

Fig. 8. Residuals and time evolution of the pointwise temperature at the bottom of the plate.

4.3. A full three-dimensional computational model

The final analysis of this configuration is performed using a comprehensive computational model that accounts for the full three-dimensional physics of the problem. In this case, the geometry of the plate is updated to include the nozzle previously presented, positioned at the upper part of the plate. The nozzle is designed to spray water onto the surface in order to ensure complete coverage and, consequently, effective thermal shielding. Given the need to implement a complex and robust computational model, the plate dimensions were reduced from 0.5×2.5 m to 0.5×0.5 m. Subsequently, in the section concerning model validation, the plate was extended to its actual size to achieve results consistent with the experimental data. The first part of this study involved a detailed analysis of the fluid dynamics; therefore, the energy equation was neglected as an initial assumption in order to simplify the model and reduce the computational cost. To define the fluid-dynamic setup, the focus was placed on the jet distribution and on accurately solving the flow equations [13,15]. Once a robust model was established, the thermal equations were introduced and subsequently analysed in the section dedicated to model validation.

The fluid-dynamic setup involves the implementation of the Volume of Fluid (VOF) model, which is typically employed in applications where two Eulerian phases (e.g., water/air) interact with each other. This approach is particularly suitable for simulations involving [13,15]:

- water jets sprayed in open environments;
- tanks containing multiple fluid phases that mix;
- other applications requiring accurate tracking of the interface between immiscible phases.

Firstly, knowing the reference flow rate and the characteristic dimension of the nozzle, which has a diameter of 3.6 mm, the fluid flow was modelled as turbulent. The realizable k-ε turbulence model was adopted due to its robustness and numerical stability for high-Reynolds-number jet impingement flows. Although alternative models such as the SST k-ω could also be employed, they typically require very low y^+

values and a significantly finer near-wall prism layer, resulting in increased computational cost. The k-ε model therefore represents a more efficient choice, consistent with the objective of achieving an optimal balance between accuracy and computational efficiency. [13,20]. Indeed, turbulence was also taken into account during mesh generation [15]. As shown in Fig. 9, a boundary layer was introduced to capture turbulence near the wall, where strong velocity gradients occur. The number of layers and the thickness of the boundary layer, as well as the thickness of the first layer near the wall, were selected to ensure a low y^+ value [15]. A realizable k-ε two-layer model with a two-layer all y + wall treatment was employed; this model performs well at both low and high y^+ values. In this case, a low y^+ was preferred to achieve higher accuracy in resolving the near-wall turbulence [13,15,20].

Although the two phases (water/air) interact in the VOF model, surface tension effects must also be considered. This aspect was critical during the model definition stage. Theoretically, the simulation should have been performed in transient conditions while accounting for surface tension; however, due to the high computational cost and the geometrical complexity, the problem was simplified by neglecting surface tension and setting the simulation in steady-state conditions. This simplification is supported by analytical considerations based on the Weber number (defined in Eq. (3), which represents the ratio between inertial forces and surface tension forces. For high Weber numbers, inertial forces dominate the problem, making surface tension effects negligible and thus justifying the adopted approach [21].

$$We = \frac{\rho v^2 L}{\gamma} \tag{3}$$

where ρ is the fluid density, v is the velocity, L is the characteristic length, and γ is the surface tension between the two fluids. Moreover, Tab. 3 reports the main dimensionless groups governing the system, both for the CFD simulations and for the MATLAB code used to solve the fluid-dynamic equations.

When the Weber number We ≫ 1, the effect of surface tension can be neglected, as inertial forces are dominant. Conversely, for We ≪ 1, surface tension plays a significant role in the dynamics of the phenomenon. This behaviour is consistent with physical intuition: at low velocities (low We values), surface tension governs the formation of nearly spherical droplet geometries and their distribution; at high velocities (high We values), the dynamics are primarily controlled by flow inertia, making surface tension a secondary effect. In the present study, since the Weber number is directly proportional to the square of velocity, this was calculated to ensure We ≫ 1 [21]. From this analysis, a threshold value of approximately 0.02 m/s was obtained. Therefore, for velocities greater than this value, surface tension can be considered negligible and

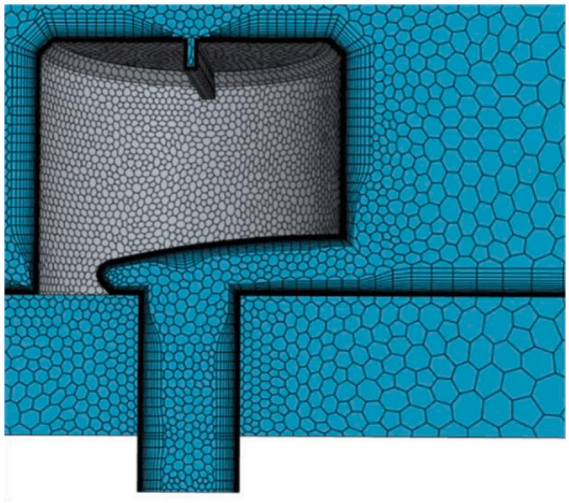

Fig. 9. Mesh setup for the CFD VOF simulation.

Table 3
Dimensionless numbers governing the thermo-fluid dynamic problem.

Dimensionless number	Definition	Physical interpretation
Reynolds number (Re)	$Re = \frac{\rho v L}{\mu}$	Ratio between inertial and viscous forces; defines the flow regime (laminar/turbulent) of the impinging jet
Prandtl number (Pr)	$Pr = \frac{c_p \mu}{k}$	Ratio between momentum and thermal diffusivity; characterizes heat transfer in the fluid
Nusselt number (Nu)	$Nu = \frac{hL}{k}$	Dimensionless heat transfer coefficient; represents the efficiency of convective heat transfer
Weber number (We)	$We = \frac{\rho v^2 L}{\gamma}$	Ratio between inertial and surface tension forces; used to assess the relevance of surface tension effects

excluded from the computational model. Indeed, in the configuration analysed in this work, given the nozzle geometry and the target flow rate, the estimated velocity is much higher, thus confirming the assumption of neglecting surface tension. This simplification also allowed the problem to be set under steady-state conditions. Surface tension introduces inherently transient and unstable effects; once removed, the solver was able to reach a numerically stable condition closer to stationarity. It is worth noting that, since the physical phenomenon is inherently unsteady and unstable by nature, this approach does not provide a complete physical description of the process. Nevertheless, it represents an effective compromise between accuracy and computational cost, sufficient to reproduce the jet distribution at the nozzle outlet. Furthermore, the analysis was conducted by simulating half of the plate and applying a symmetry condition. This approach was feasible because both the nozzle and the plate exhibit symmetry with respect to the central axis, which further reduced computational cost and accelerated the simulation time. Fig. 10 shows the four simulations performed with increasing velocity and, consequently, increasing Reynolds number [17]. All four cases satisfy the minimum threshold condition required to ensure We ≫ 1. Moreover, test 4 is conducted under the same fluid-dynamic conditions shown in section 4.1 and 4.2, with a Reynolds number of approximately 50000. As shown, increasing the velocity results in a longer jet and, consequently, a wider distribution [15]. This behaviour is consistent with the assumptions made in the section of the fluid film model: after an initial impact region, the flow stabilizes, forming a continuous film that flows along the plate. Furthermore, these results highlight the flow instability mentioned earlier. For instance, in the region immediately adjacent to the jet impact, a curvature forms due to the backflow of water on the wall. This is actually caused by forcing the simulation into a single steady-state condition, thereby neglecting the time-dependent dynamics. However, the constant shape of the fluid after the impact zone computationally confirms the possibility of approximating the complex physics of the problem using the model presented in Section 4.2, thereby reducing both computational cost and required simulation time. Finally, since the main goal is not the jet fluid dynamics but the investigation of thermal shielding, the multiphase VOF model was compared with the fluid film model (Sec. 4.2) in order to evaluate the thermo-fluid dynamic results and validate the proposed approximation.

5. Validation of the computational model

After defining in detail the three fluid-dynamic models for describing the problem, experimental tests were conducted to validate the accuracy of the setup and the computational calculations. The tests were performed on a plate with the same characteristics previously described: dimensions of 0.5 m × 2.5 m, thickness of 5 mm, and an inclination of 45°. Additionally, realistic operating conditions were replicated, including the initial temperature profile and the solar heat flux measured for that specific experiment.

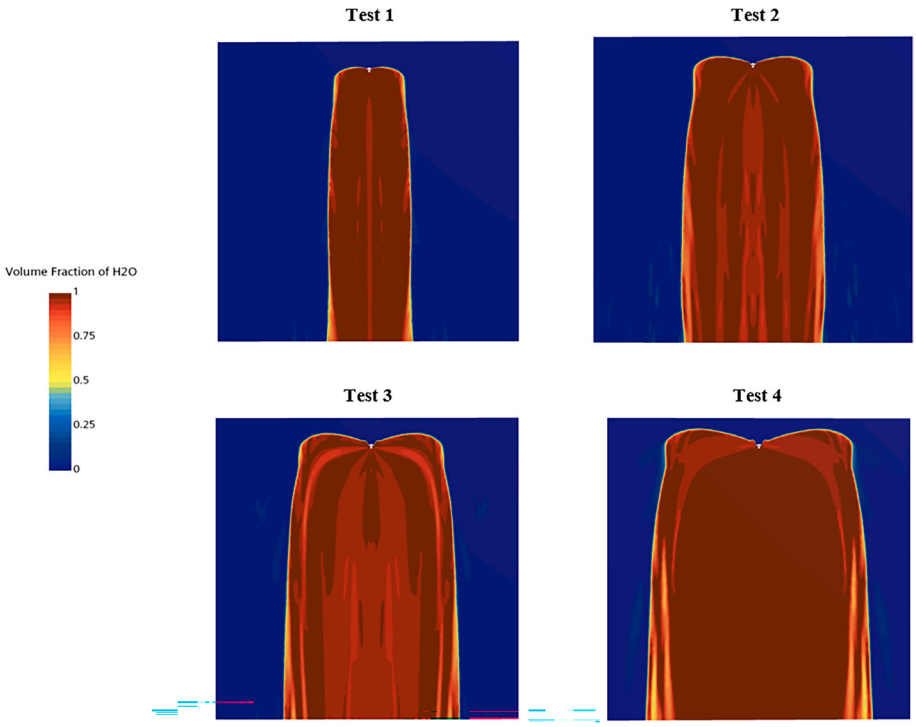

Fig. 10. Water jet distribution as a function of inlet velocity.

Furthermore, two types of coating were used on the plate:

- A standard coating characterized by an estimated absorption coefficient of 75% (a).
- A commercial low solar absorbing coating with an estimated absorption coefficient of 57% (b).

Both cases (a and b) were analysed to validate the fluid-dynamic model. For the boundary conditions, the initial temperature profile was obtained from experimental measurements. Specifically, five temperature probes were positioned on the plate, and the recorded data were interpolated in MATLAB to reconstruct an approximate thermal profile along the entire plate. Fig. 11 shows the plate with the locations of the measurement points, and the corresponding values are reported in Table 4. Since the positions of the probes were constrained by the experimental setup, the temperature sensors in the CFD simulations were placed at the same locations to ensure a consistent and direct comparison between experimental and numerical results. The experimental setup and the measurement campaign are discussed in greater detail in the following section. Finally, future work will focus on increasing the number of probes and acquiring temperature data at more spatially distributed locations to further improve the comparison grid between experimental and numerical results.

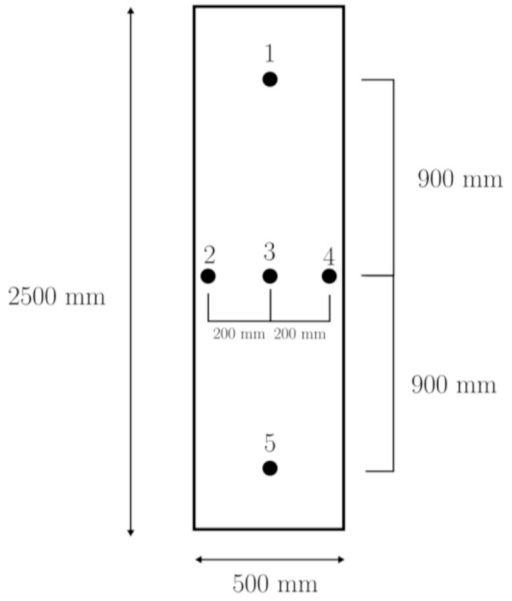

Fig. 11. Schematic representation of the plate showing the experimental measurement points.

5.1. Experimental campaign

The experimental campaign was conducted using a rigid frame containing two plates, each measuring 0.5 m × 2.5 m, inclined at 45°. The first plate was coated with standard paint (75% solar absorption coefficient), and the second with low solar absorption (LSA) paint (57% absorption coefficient). Both the standard-paint and LSA-coated plates were equipped with nozzles. The nozzle was positioned at the top edge of each plate, aligned with the upper boundary, in a configuration consistent with the numerical model. This position ensured that the water film developed along the plate under the combined effects of gravity and jet impingement, reproducing the same flow initiation conditions in both the experimental and computational analyses. The nozzle also exhibited the same geometric characteristics as those previously illustrated in Fig. 2, ensuring geometric consistency between the experimental and numerical configurations. Its specific design produced a fan-shaped jet, allowing uniform water distribution across the plate

Table 4
Initial temperature measured at the points shown on the plate for the two proposed coating configurations.

T [°C]	1	2	3	4	5
Coating (a)	27.2	29	31.8	27.9	30.7
Coating (b)	26.9	27.9	25.2	28	27.1

width and promoting the formation of a continuous and stable liquid film along the inclined surface. Water was supplied to the nozzles via a piping system incorporating a flow meter and a thermocouple, the latter used to measure the incoming water temperature. The operating conditions were defined based on the experimental constraints. In this first experimental campaign, the water temperature at the nozzle outlet was maintained at 26°C, while the flow rate was continuously monitored using a calibrated flow meter and maintained constant throughout each experimental run to guarantee reproducibility of the turbulent flow conditions, with a Reynolds number of approximately 50000. The incident solar heat flux was experimentally measured and averaged at 840 W/m^2 during the tests. Each plate was instrumented with five thermocouples, enabling the measurement of temperature evolution over time at multiple locations. Temperature was measured using a type T thermocouple (copper-constantan), IEC 60584 class 1 accuracy, with grounded junction. The probe consisted of an AISI 316 L stainless steel sheath (4.5 mm diameter, 20 mm length) connected to a 10 m twisted cable insulated with silicone rubber (maximum operating temperature 200°C). A stainless steel foil was welded along the sheath to improve thermal contact with the measured surface. The thermocouples were welded to the dry surface of the plates, i.e., the surface opposite to that exposed to the water jet. This configuration does not compromise the validity of the measurements, as the temperature gradient across the thin thickness of the plate can be considered negligible. Each experimental cycle followed a repeatable procedure. Initially, the plate was exposed to solar radiation and allowed to heat until the prescribed initial temperature distribution was reached. Once the desired initial condition was reached, the water jet was activated and maintained for several minutes to ensure that the plate reached steady-state conditions. Simultaneously, the thermal results were recorded using a thermal imaging camera, the measurement characteristics of which are summarized in Table 5. Finally, the water jet was turned off and the system was allowed to return to its initial state, thus starting a new cycle. Fig. 12 presents a schematic representation of the experimental setup, showing (a) the side view and (b) the front view. The optical configuration used for the measurements provided a field of view (FOV) of 24° × 18°, ensuring proper framing of the targets in both vertical and horizontal directions while maximizing the spatial resolution. The infrared (IR) camera was positioned at a distance of 5 m from the target, resulting in a spatial resolution of approximately 6 mm per pixel on the observed surface. This resolution enabled accurate correspondence between the experimental measurement points and the extraction points in the CFD model.

Since the experimental campaign was conducted outdoors, atmospheric conditions would have influenced the thermal response of the plates. Variations in solar radiation due to cloud cover, ambient air temperature, and wind speed act as uncontrollable and weather-dependent boundary conditions, inevitably leading to small discrepancies between different sets of experiments. Therefore, the experiments were conducted under carefully controlled outdoor conditions to minimize disturbances. Following the collection of experimental data, numerical simulations were performed using the corresponding boundary conditions, aiming to replicate the experimental setup and operating conditions as faithfully as possible. Finally, the thermal results of the multiphase VOF and the fluid-film model are first compared, to highlight the small discrepancies between the results. Subsequently, the CFD analysis and fluid-film model is validated by comparison with the thermal measurements recorded during the experimental campaign.

Table 5
Thermal imaging camera characteristics and measurements uncertainty for experimental studies.

Measurement	
Temperature range	• From −20°C to 120°C • From 0°C to 650°C • Optionally from 300°C to 1000°C
Precision	From −20°C to 120°C: From 0°C to 650°C: Optional range from 300°C to 1000°C: ±2% • From −20°C to 100°C: ±2°C • From 100°C to 120°C: ±2°C • From 0°C to 100°C: ±2°C • From 100°C to 650°C: ±2°C

5.2. Comparison between the fluid film and VOF models

The tests were conducted under an incident solar heat flux of 840 W/m^2, with an inlet water flow rate maintained at a constant value and a temperature of 26°C. First, the fluid-film computational model was compared with the three-dimensional multiphase model implementing the VOF approach [15]. As shown in Fig. 13, the thermal results at selected characteristic points were analyzed for both models. The graphs present the temperature along the centerline of the plate at points 1, 3, and 5, as well as the temperature values on the right and left sides of the plate at points 2 and 4. These results indicate that the central region exhibits nearly identical thermal behaviour in both models, with the minor differences likely attributable to model approximations and numerical accuracy. At the lateral points, the fluid-film model shows a uniform temperature between the right and left sides, as the water descends linearly along the plate. In contrast, the VOF simulation displays different temperatures at the right and left sides due to the jet dynamics and turbulence. In this case, because the initial temperature field was not symmetric, the VOF simulation was performed without applying symmetry, and the plate length was extended to 2.5 m to obtain results that are realistic and comparable with the experimental data.

The maximum temperature difference between the fluid-film and VOF models was evaluated as a quantitative comparison criterion. The largest difference of 1.2°C occurs at the lateral points 2 and 4, while along the centerline the maximum difference is only 0.16°C. These values are relatively small, and focusing on the central region, where jet-induced asymmetry is negligible, the two models yield practically identical results.

Therefore, it can be concluded that the fluid-film model allows the thermal problem to be solved more efficiently and straightforwardly. This approach enables the transient thermal history of the plate to be analysed while significantly reducing computational time and achieving convergence within practical limits [16]. Moreover, the model can be readily adapted to larger plate geometries without incurring excessive computational cost. Since the study does not focus on microscopic droplet dynamics or other phenomena governed by surface tension, the fluid-film approximation reliably captures the thermal behaviour while maintaining nearly identical results to the full VOF model.

Finally, although the fluid-film model produces results very similar to those of the one-dimensional MATLAB model, it is preferred over the analytical approach because it provides a more detailed representation of the fluid dynamics, accounting for the local heat transfer coefficient as a function of plate geometry, inclination, and boundary conditions.

5.3. Comparison between the fluid film and experimental data

Once the accuracy of the fluid-film approximation was demonstrated, the computational model was validated through comparison with the data collected during the experimental campaign.

The primary objective was to validate the model, ensuring a reliable thermo-fluid dynamic design for the engineering-scale up of the plate. Once proven effective at small scale, the same setup can be applied to larger geometries, enabling the analysis of thermal profiles in configurations that are not feasible to test experimentally.

The simulations were conducted by applying the boundary conditions used during the experimental tests:

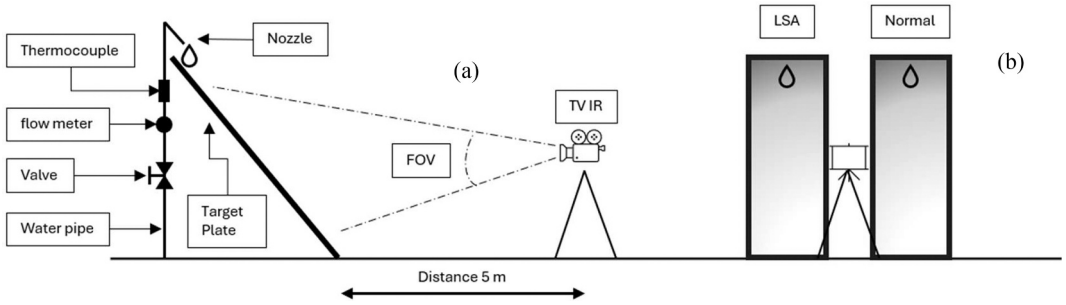

Fig. 12. Schematic representation of the experimental setup showing (a) side view and (b) front view, including the infrared camera position, target location, and measurement distance.

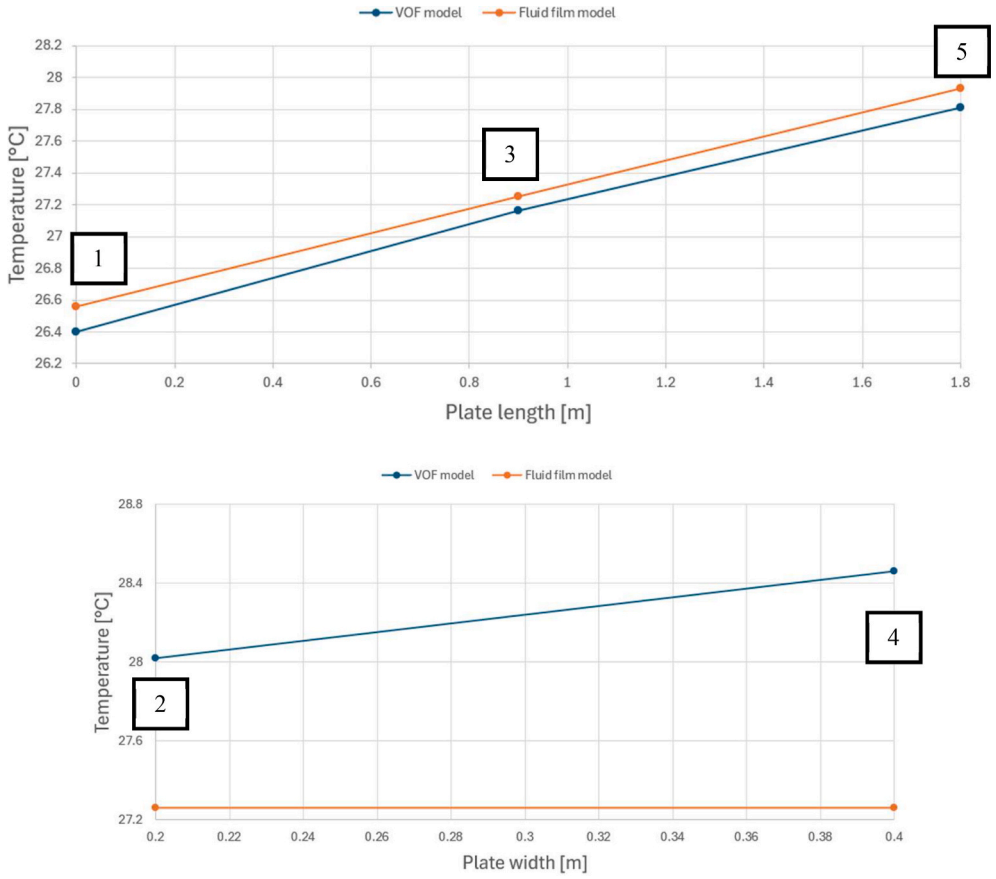

Fig. 13. Comparison of the temperature profile between the VOF and fluid film models along the plate length and width, taking as reference the points experimentally measured during the tests.

- A mass flow rate consistent with the experimental conditions and sufficient to ensure a Reynolds number of approximately 50000, at a temperature of 23°C.
- Initial plate temperature profile set by interpolating the five points measured with thermocouples on the actual plate.
- Thermal power of 840 W/m^2, considering the two coating configurations (a) and (b) described previously in section 5.

Two simulations were performed considering coating absorption coefficients of 75% and 57%, respectively. From a thermal perspective, these differences lead to variations in absorbed power, resulting in correspondingly higher or lower plate temperatures. As expected, the higher the absorbed power, the higher the temperature attained by the plate. To minimize plate temperature, a coating with high solar reflectivity should be selected. Fig. 14 presents the temperature profiles obtained from the CFD simulations, compared with the experimental data. Profiles along the plate at points 1, 3, and 5, as well as across the width of the plate at points 2 and 4, are shown for both coating configurations (a) and (b).

Again, from these results, the difference between the experimentally measured temperature and the temperature predicted by the CFD model was calculated, showing a maximum deviation of 1.31°C for case (a) and 0.95°C for case (b). For both cases, the mean absolute error (the ratio between the sum of the temperature differences for the five points and the number of points) was also evaluated, resulting in 0.79°C and 0.59°C, respectively. The results remain within a 10% deviation, thus confirming the good accuracy of the proposed setup.

It should be noted that the data discrepancy is sensitive to the testing campaign, including atmospheric conditions, temperature field acquisition, and boundary conditions such as thermal power, actual inlet

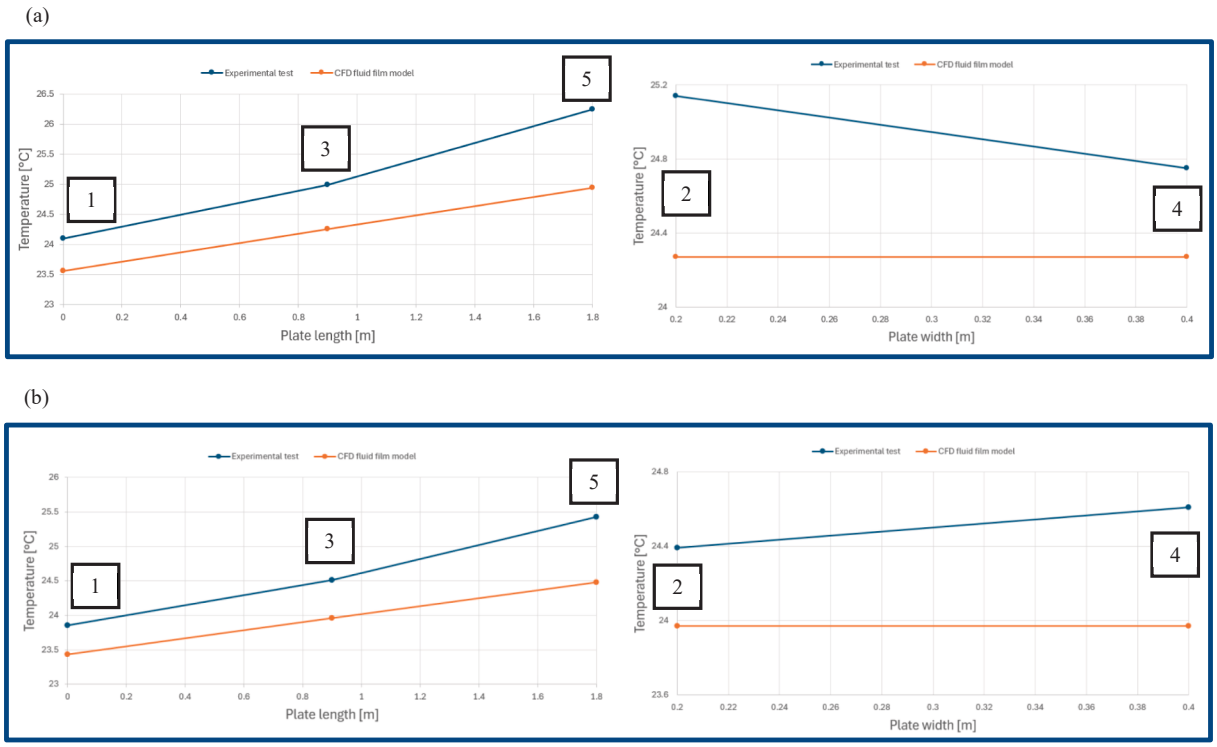

Fig. 14. Comparison of the temperature values at the measurement points between the experimental tests and the fluid film CFD model, for both coating configurations (a) and (b).

temperature, and heat losses in the pipes transporting water to the nozzle exit, as well as the intrinsic accuracy of the measurement equipment.

Therefore, assuming a maximum error threshold of 10% is reasonable in this case. Overall, it can be concluded that the fluid-film model reproduces the trend observed in the experimental data, with temperature values in excellent agreement.

Finally, the results presented in this study highlight the role of the main governing parameters on the thermo-fluid dynamic behaviour of the jet-cooled inclined plate. The Reynolds number, set to approximately 50,000 to match experimental conditions, ensures a fully turbulent flow regime, justifying the adoption of a RANS-based turbulence modelling approach. At the same time, the high Weber number confirms that inertial forces dominate over surface tension effects, supporting the modelling assumption adopted in the VOF simulations.

From a modelling perspective, the comparison between the one-dimensional, fluid film, and multiphase VOF approaches shows that the overall thermal response of the plate is primarily governed by the macroscopic flow and heat transfer mechanisms, rather than by detailed jet atomization effects. This explains the close agreement observed between the simplified fluid film model and the more complex VOF simulations, particularly in terms of mean temperature distribution.

The absorbed heat flux and coating properties directly affect the steady-state temperature levels, while the plate inclination influences the development of the water film through gravity-driven flow. The combined analysis of these parameters confirms that the proposed modelling approach captures the dominant physical mechanisms governing the system and provides reliable predictions under the investigated operating conditions.

6. Conclusions

The study presented in this work provided a detailed thermo-fluid dynamic analysis aimed at investigating the washing efficiency and thermal shielding of an inclined plate, which is representative of nozzle cooling systems in industrial applications. Three fluid dynamic models of increasing complexity were analyzed, ranging from a one-dimensional model implemented in MATLAB to compact three-dimensional CFD models solved in STAR-CCM + . The main contribution of this research consists in the systematic comparison between the fluid film and VOF-CFD approaches, combined with experimental validation, in order to evaluate the trade-off between computational cost and predictive accuracy in spray cooling and washing applications. While recent studies in the literature have primarily focused on detailed CFD modeling or experimental investigations of impingement and spray cooling systems, the present work demonstrates that the simplified fluid film approach is capable of predicting the thermal behavior with accuracy comparable to the more computationally expensive VOF model. This represents a significant advancement, as it provides a reliable and computationally efficient methodology for the simulation and design of cooling systems.

The comparison between the fluid film and VOF models showed that both approaches produce nearly identical thermal results, allowing the physical problem to be simplified without compromising accuracy. This enables a significant reduction in computational cost, making the fluid film model particularly suitable for engineering applications involving parametric studies, optimization, and system-level simulations.

Furthermore, the computational results were validated against experimental measurements, showing good agreement and confirming the accuracy and robustness of the developed thermo-fluid dynamic framework. This validation strengthens the reliability of the proposed modeling approach and its applicability to real industrial cooling systems.

The findings of this study contribute to the advancement of thermal science and engineering by providing a validated and computationally efficient methodology for modeling spray cooling and liquid film thermal shielding, which are critical aspects in the design and optimization of thermal management systems.

Future research will focus on extending the developed methodology to transient operating conditions, different geometrical configurations,

and varying boundary conditions, as well as integrating the simplified modeling approach into system-level design and optimization tools. These developments will support the design, control, and optimization of advanced cooling systems with improved thermal performance and reduced computational requirements.

CRediT authorship contribution statement

Alfredo Pagliaro: Conceptualization. **Francesco Braghin:** Supervision. **Francesco Devia:** Supervision. **Gregorio Giannini:** Writing – review & editing, Writing – original draft, Supervision. **Vittoria Malaman:** Writing – review & editing, Writing – original draft, Supervision. **Francesco Miselli:** Writing – review & editing, Supervision.

Declaration of competing interest

The authors declare that they have no known competing financial interests or personal relationships that could have appeared to influence the work reported in this paper.

Acknowledgements

This work was carried out in collaboration with Fincantieri S.p.A. and the University of Genoa. We would like to thank all colleagues who contributed to this study for their invaluable support.

Data availability

The data that has been used is confidential.

References

[1] H. K. Versteeg, *et al.*, "An Introduction to Computational Fluid Dynamics: The Finite Volume Method (2nd ed.)", *Pearson Education*, 2007.
[2] A. Y. Tong, "Impingement Heat Transfer of Free-Surface Liquid Jets", *ASME 2002 International Mechanical Engineering Congress and Exposition,* Jun. 2008, doi: 10.1115/IMECE2002-39396.
[3] B. Singh, *et al.*, "Performance Enhancement of Solar Photovoltaic Cooling Using Water Sprinkler", *International Journal of Engineering & Technology*, Jan. 2018, 7 (4.18) (2018) 32-37.
[4] B. Bird, "Transport Phenomena", 2001.
[5] I. Mudawar, "Assessment of High-Heat-Flux Thermal Management Schemes", *IEEE TRANSACTIONS ON COMPONENTS AND PACKAGING TECHNOLOGIES*, vol. 24, no.2, Jun. 2001, doi:10.1109/6144.926375.
[6] J. Kim, Spray cooling heat transfer: the state of the art, Int. J. Heat Fluid Flow 28 (2007) (Nov. 2006) 753–767, https://doi.org/10.1016/j.ijheatfluidflow.2006.09.003.
[7] A. Karabey, et al., Optimization of the Design Parameters using the Taguchi Method In Inclined Impingement MultiJet Heat transfer with Rectangular Finned Heat Sink, Heat Transfer Res. 54 (Mar. 2023) 37–51, https://doi.org/10.1615/HeatTransRes.2023046672.
[8] A. Karabey, et al., Numerical Determination of Cooling Performance on Heat Sink using Impingement Jet, Journal of Science & Technology 11 (2023) 977–989, https://doi.org/10.29130/dubited.1076314.
[9] A. Karabey, *et al.*, "Experimental and Numerical Investigation of Flow and Heat Transfer Characteristics Using Jet Impinging on Optimized Rectangular Finned Heat Sinks", *Heat Transfer Research*, vol. 53, pp. 61-77, May. 2022, doi: 10.1615/HeatTransRes.2022042480.
[10] A. Karabey, et al., Analyzing the Heat and Flow Characteristics In Spray Cooling by using an Optimized Rectangular Finned Heat Sink, Heat Transfer Res. 55 (Feb. 2024) 19–34, https://doi.org/10.1615/HeatTransRes.2024051370.
[11] R. Erdin, *et al.*, "Experimental and Numerical Comparison of Heat and Flow Characteristics of Concave Heat Sink in Cooling with Multi-Impinging Air Jet", *Journal of Energy Trends*, 2(2), 62-72, doi: 10.5281/zenodo.18334301.
[12] L. Cappon, et al., Study of the cooling of a metal plate at high temperature by water spraying, J. Phys. Conf. Ser. 2885 (2024) 012080, https://doi.org/10.1088/1742-6596/2885/1/012080.
[13] Siemens CD-adapco. *STAR-CCM+ User Guide.* 2020.
[14] N.K. Kund, Experimental Exploration on Influences of Nozzle to Plate Spacing on Cooling Performances using Impinging Water jets, International Journal of Innovative Technology and Exploring Engineering (IJITEE) 8 (Oct. 2019), https://doi.org/10.35940/ijitee.L2913.1081219.
[15] M.R. Guechi, et al., On the numerical and experimental study of spray cooling, The Journal of Computational Multiphase Flows 5 (Dec. 2013), https://doi.org/10.1260/1757-482X.5.4.239.
[16] J. Ondrouskova, et al., Nozzle Cooling of Hot Surfaces with Various Orientations, The European Physical Journal Conferences (Apr. 2012), https://doi.org/10.1051/epjconf/20122501063.
[17] A. Karabey, et al., Experimental Analysis of Heat and Flow Characteristics on Inclined and Multiple Impingement Jet Heat transfer using Optimized Heat Sink, Appl. Sci. 15 (Mar. 2025) 2657, https://doi.org/10.3390/app15052657.
[18] N.K. Kund, Comparative CFD Studies on Jet Impingement Cooling using Water and Water-Al2O3 Nanofluid as Coolants, International Journal of Innovative Technology and Exploring Engineering (IJITEE) 8 (May 2019).
[19] S.V.R. Bandaru, et al., Multi-nozzle spray cooling of a reactor pressure vessel steel plate for the application of ex-vessel cooling, Nucl. Eng. Des. 375 (Apr. 2021), https://doi.org/10.1016/j.nucengdes.2021.111101.
[20] R.D. Plant, et al., A review of jet impingement cooling, International Journal of Thermofluids 17 (Feb. 2023), https://doi.org/10.1016/j.ijft.2023.100312.
[21] A. H. Lefebvre, *et al.*, "Atomization and Sprays (2nd ed.) ", *CRC Press*, 2017.